Composition, nanostructure, and optical properties of silver and silver-copper lusters

Trinitat Pradell,[1] Radostin S. Pavlov,[1] Patricia Carolina Gutiérrez,[2] Aurelio Climent-Font,[2] and Judit Molera[3]

[1]*Center for Research in NanoEngineering, Universitat Politècnica de Catalunya and Departament de Física i Enginyeria Nuclear, Universitat Politècnica de Catalunya, Campus Baix Llobregat, ESAB, Esteva Terrades 8, 08860 Castelldefels, Barcelona, Spain*
[2]*Centro de Micro-Análisis de Materiales, Universidad Autónoma de Madrid, 28049 Madrid, Spain and Departamento de Física Aplicada, C-XII, Universidad Autónoma de Madrid, Campus de Cantoblanco, 28049 Madrid, Spain*
[3]*GRTD, Escola Politècnica Superior, Universitat de Vic. C. de la Laura, 13, 08500 Vic, Spain*

Lusters are composite thin layers of coinage metal nanoparticles in glass displaying peculiar optical properties and obtained by a process involving ionic exchange, diffusion, and crystallization. In particular, the origin of the high reflectance (golden-shine) shown by those layers has been subject of some discussion. It has been attributed to either the presence of larger particles, thinner multiple layers or higher volume fraction of nanoparticles. The object of this paper is to clarify this for which a set of laboratory designed lusters are analysed by Rutherford backscattering spectroscopy, transmission electron microscopy, x-ray diffraction, and ultraviolet-visible spectroscopy. Model calculations and numerical simulations using the finite difference time domain method were also performed to evaluate the optical properties. Finally, the correlation between synthesis conditions, nanostructure, and optical properties is obtained for these materials. © *2012 American Institute of Physics*. [http://dx.doi.org/10.1063/1.4749790]

I. INTRODUCTION

Luster is a coinage metal nanoparticles-glass composite displaying peculiar optical properties. The most remarkable feature of these materials is their high specular reflectance conveying to them metal-like appearance.[1–4] Although all this may suggest a product of modern nanotechnology and engineering, the fact is that the first lusters were obtained as early as 9th century A.D. in the Abbasid caliphate.[5,6]

Several studies have shown that the lusters consist of a thin surface layer (several hundred nanometers thick) of metal nanoparticles, silver and/or copper with sizes ranging between 2 and 50 nm, randomly distributed within a glassy matrix.[1–4] The production process[7–9] involves first ion exchange between the silver/copper ions (Ag^+/Cu^{2+} or Cu^+) from an initial mixture applied on the glass surface and the alkaline (Na^+ and K^+) ions from the glass, and then the nucleation and growth of metal nanoparticles through reduction of Ag^+ to Ag^0 and Cu^{2+}/Cu^+ to Cu^0.

Differences in both specular reflectance and color of lusters are related to the localized absorption (surface plasmon resonance, SPR) and scattering (Mie scattering) of the visible light by the metal nanoparticles, which depend on their size, shape, and concentration.[10] Spherical silver nanoparticles absorb and scatter strongly in the blue region of the spectra (around 400–450 nm) but are essentially transparent to the rest of the wavelengths in the visible and this causes the typical greenish-yellow color of silver colloidal solutions. The SPR absorption band (at 560 nm) and electronic inter-band transitions absorbing at shorter wavelengths of copper nanoparticles confer red hues to copper colloidal solutions. The

presence of cuprite (Cu_2O) nanoparticles (absorption at about 520 nm) and of copper ions (Cu^+ and Cu^{2+}) dissolved in the glass modifies the color shown by the luster layers.[11,12] Finally, increasing the size of the metal nanoparticles or the refraction index of the glassy matrix red shifts the SPR absorption bands and, consequently, also varies the color of the luster layer.

On the other hand, with increasing the nanoparticles volume fraction, the optical spectra are modified even further and cannot be attributed anymore to scattering by individual particles (Mie scattering) but should rather be considered as the result of collective scattering by an ensemble of particles.[13,14] This type of scattering has been observed in many different systems;[15,16] such materials are essentially composites consisting of organic dielectric materials and show intense colors and strong reflectance. The corresponding structures can be formally divided into ordered and disordered ones and can be treated as photonic crystals and photonic glass, respectively. Lusters resemble especially the latter case, but differ from it in that the metal spheres suspended in the glass are much smaller and their dielectric function has a large imaginary part which is why they not only scatter but also absorb strongly.

Recent laboratory replication of copper lusters,[17] as well as the analysis of early silver Islamic lusters,[18] revealed a direct correlation between the use of a PbO containing glass and the success in obtaining the metal like shine. The addition of PbO reduces the diffusivity of copper and silver in the glass and consequently helps the development of more superficial and thinner luster layer containing a higher volume fraction of an often bimodal size distribution of larger

112, 054307-1

nanoparticles. Although, there is no doubt that this complex nanostructure is responsible for the metal like appearance of luster, there is still controversy about which of the above-mentioned factors is the most important: the presence of larger metal nanoparticles,[19] the high volume fraction of particles,[7,17,18] the bimodal particle size distribution,[20] or the alternation of layers with different thickness and volume fraction of particles.[21,22] In fact, red non-coppery luster layers produced on a lead free glaze were thick (800 nm) and formed by 10 nm copper nanoparticles.[23] On the contrary, the coppery luster layers produced over PbO containing glazes following the same protocol were thin (150 nm)[17] and contained large (50 nm size) and small (a few nanometers size) copper nanoparticles. Therefore, it was not possible to elucidate which of the factors or combination of the factors was responsible of the metallic appearance.

In order to clarify the role of the nanoparticles size and luster layer thickness in the final "golden shine" achieved by silver lusters, a set of laboratory-made silver lusters were designed in order to obtain similar nanoparticle size distributions and layer thicknesses, but different volume fractions of the nanoparticles. Copper-containing silver lusters were also obtained to confirm the role of copper in the color shown by the layers and also on the development of the bluish and purplish shine observed. The chemical composition, metal volume fraction and thickness of the luster layers and the nature and size of the nanoparticles were determined and related to their color and specular reflectance.

The final goal of the study is to determine the correlation between parameters and materials employed, nanostructures obtained and the resulting color and reflectance. For this, absorption and scattering spectra are modeled by Mie scattering and mean field models[13,14] and also, taking into account the inherent complexity of multiparticle collective scattering, a numerical method to solve Maxwell equations for complex systems with almost arbitrary geometrical configuration, (finite difference time domain, FDTD).[24] The production of composite thin layers of coinage metal nanoparticles in glass has a number of applications provided that the thickness, composition, size, and volume fraction of the particles are controlled. Properties such as dichroism and wavelength dependent reflectance and absorbance can find application in the field of optoelectronics and solar cells. The study suggests mechanisms for tailoring the optical properties through control of the nanostructure and therefore may be of interest to those fields.

II. MATERIALS AND TECHNIQUES

The samples were obtained by applying a copper and/or silver-containing mixture over glazed ceramic supports, which were afterwards submitted to a heat treatment first in neutral and then in reducing atmosphere as already described elsewhere.[7] Thermal protocols consisted in a heating ramp at a rate of $50\,^{\circ}C/min$ and slow argon flow (5 ml/min) until reaching a temperature of $550\,^{\circ}C$, followed by reduction at constant temperature in a 95%Ar + 5%H$_2$ mixture during 30 min for j126, j6, and j65, but only 10 min for r254. Samples k14 and k17 were produced following a similar thermal

protocol but using a mixture of N$_2$ + CO (90:10) as a reducing gas and heating to higher firing temperatures of $600\,^{\circ}C$.[25] It was found that this gas mixture is not suitable for the production of a pure copper luster, while it is adequate for silver and silver-copper luster production. All samples were cooled down to room temperature in less than 10 min.

Samples j126, j6, k14, and k17 were obtained over a lead-free glaze (glaze A) while r254 and j65 were obtained over a lead-bearing glaze (glaze AL) obtained by mixing the lead-free glaze with a high lead content glaze (70% PbO). The chemical composition[7] of the lead-free glaze is 48.5% SiO$_2$, 12.0% Na$_2$O, 7.1% K$_2$O, 23.3% B$_2$O$_3$, 7.2% Al$_2$O$_3$, 0.9% CaO, and 0.1% MgO; while that of the lead bearing glaze is 43.5% SiO$_2$, 3.5% Na$_2$O, 2.9% K$_2$O, 11.0% B$_2$O$_3$, 5.7% Al$_2$O$_3$, 31.8% PbO, 0.9% CaO, and 0.1% MgO. The density and refractive index of both glazes were calculated from the glaze compositions using the expressions given by Fluegel[26] and Priven and Mazurin,[27] respectively, and are shown in Table I.

Rutherford backscattering spectroscopy (RBS), x-ray diffraction (XRD), transmission electron microscopy (TEM), and ultraviolet-visible spectroscopy (UV-Vis) were performed in order to determine the composition, size distribution, and volume fraction of metal nanoparticles in the luster layers.

RBS measurements[28] were performed on the 5 MV tandem accelerator.[29] A 3035 keV energy He-beam with square-section (1 mm in diagonal) was used thus taking advantage of the elastic resonance $^{16}O(\alpha,\alpha)^{16}O$ occurring at this energy[30] and increasing the sensitivity to oxygen concentration by a factor of 23. The samples were kept in vacuum. The backscattered ions were analyzed by means of two surface-barrier particle detectors, one fixed at 170° scattering angle and another at an adjustable scattering angle. The scattering angle of the mobile detector was determined from a database listing the scattering angles and scattering cross sections for each elastic resonance. For the current measurements, the angle of the adjustable detector was set at 165°. Normally both detectors were used simultaneously so that the RBS spectra obtained by each one are validated with the other one. A careful quantification was performed by employing the simulation code SIMNRA.[31]

RBS data were fitted starting from the average chemical compositions obtained from microprobe analysis of the layers and following a procedure described elsewhere.[17,18] Similar procedures have been employed for fitting the RBS data from historical lusters.[32–34]

To determine the luster depth composition profiles, a sequence of layers with varying silver and/or copper content was modeled. The depth concentration profiles of the luster layers were fitted using between 10 and 15 layers of varying

TABLE I. Glaze properties calculated from their composition.

Glaze	wt. % PbO	Refraction index[a] (n)	Density[b] (g/cm^3)
A	<0.5	1.53	2.36
AL	31.8	1.58	2.84

[a]Reference 27.
[b]Reference 26.

thickness and silver/copper content. The thickness of each layer is given in units of areal densities, which can be converted into absolute thickness provided that the mean density of the layer is known.[17,18] The mean density of the luster layer was estimated by linear interpolation from the metal nanoparticle and glaze fractions taking $10.49\,g/cm^3$ for silver, $8.89\,g/cm^3$ for copper and, for the glaze, the density calculated from the RBS fittings after Fluegel.[26]

X-ray diffraction measurements were performed on beamline BM16 of the European Synchrotron Radiation Facility (ESRF) in Grenoble. The measurements were performed in transmission geometry applying a narrow beam $(50 \times 50\,\mu m)$ with 15 keV energy $(\lambda = 0.83\,\text{Å})$ on thin (about $100\,\mu m$) slices cut out of different areas of the luster layers.

A crossbeam workstation (Zeiss Neon 40) equipped with SEM (Shottky FE) and Ga+ FIB columns was used to prepare, extract, and polish the lamellae necessary for further TEM investigation. First, the sample surface was coated with a thin protective Pt layer $(1\,\mu m)$ by ion-beam-assisted deposition; then, the lamella was cut and transferred to a TEM grid. In a final step, the lamella was thinned down to a thickness transparent to the electron beam $(<60\,nm)$. High resolution transmission electron microscopy (HRTEM) characterization was performed on a JEOL JEM-2100 Lab6 electron microscope with an operating voltage of 200 kV. The chemical composition was determined by energy dispersive x-ray spectroscopy (EDS, Inca Oxford).

UV-Vis diffuse reflectance (DR) measurements were performed directly on the surface of the samples using a UV-Vis-NIR spectrophotometer (Shimadzu 3600) equipped with ISR 3100 integrating sphere.

Finite difference time domain (FDTD) simulations were performed using FDTD Solutions by Lumerical Solutions, Inc.[35] The method employed for the present work is among the most versatile and is a widely accepted tool for obtaining numerical solutions of Maxwell equations for extremely complex systems with almost arbitrary geometrical configuration, i.e., distribution of the dielectric functions of their components.[24] The most relevant restriction for the precision of this method is the discrete Yee cell size (called so to honor the inventor[36] of the method) used for the mesh of the simulation space since its lower limit directly depends on the computer power available.

The lusters were modeled as clusters of randomly distributed non-touching silver spheres suspended in SiO_2 glass and a series of simulations were performed varying the filling factor (between 0.1% and 15%) as well as the particle size of the clusters (monodisperse distributions of particles with diameters of 10 and 30 nm). The dielectric functions of both the metal and the glass were taken from Palik.[37]

A plane-wave source was placed above a glass cube containing the nanoparticle cluster and the temporal evolution of the fields transmitted through a monitor plane placed below the cube was recorded while the one corresponding to the scattered fields was recorded for/at a second monitor plane placed above the source. The whole system was surrounded by a perfectly-matched-layer (PML) box.

The number of particles necessary to fill the cube was calculated from its volume, the volume fraction desired and

the sphere volume. On the other hand, the cube volume was optimized to allow a sufficiently large number of particles, generally several hundred to several thousands to fit into it, so as to assure that their collective scattering behavior would be clearly observed while keeping the computer power demand within reasonable limits. The latter condition is also strongly related to the discrete cell size, which must be sufficiently small compared to the sphere size. In practice, a compromise was found with a Yee-cell size in the cluster region about 15 times smaller than the particle size. Further reduction of the cell size (by using a more powerful computer cluster) could be expected to improve the precision of the simulation without substantial variations in the qualitative results presented hereafter.

Chirped broad-band plane wave pulses were employed as light source functions, thus allowing one to obtain the frequency response of the system by Fourier-transforming the temporal evolution of the fields $E(t)$ and $H(t)$. Thus, the frequency-dependent Poynting vector $S(f) = E(f) \times H(f)$ was obtained and the absorption and scattering cross-sections were calculated by integrating it over the surface of the corresponding monitors and normalizing the integral with respect to the source intensity.

III. RESULTS AND DISCUSSION

The lusters obtained are shown in Figure 1. Silver lusters are green, copper lusters are red, and copper-silver lusters are brown. The production conditions were carefully selected to aid the formation of larger nanoparticles in the silver luster obtained using the alkaline glaze so as to avoid the growth of the silver nanoparticles in the silver luster produced on the lead glaze (no reducing compound was added to the precursor mixture and it was exposed to the reducing gas for a significantly shorter time). Despite this effort, the silver luster obtained using the lead glaze, r254, had golden shine while the one obtained over the alkaline glaze, j126, did not. Finally, the copper silver lusters showed the desired bluish (k17) and purplish (k14) shine.

Composition	Sample	Glaze	Color	Shine	L*	a*	b*
Copper	j65	AL		**Coppery**	35.2	11.6	6.4
	j6	A		No	39.2	20.9	6.3
Silver	j126	A		No	59.7	2.7	35.7
	r254	AL		**Golden**	47.9	1.1	25.3
Copper & Silver	k17 yellow	A		No	53.5	-1.1	12.8
	k17 brown			**Blue**	32.5	-0.7	15.8
	k14	A		**Purple**	51.5	3.3	25.2

FIG. 1. Luster layers studied. Cie Lab* color coordinates were obtained from the UV-Vis spectra.
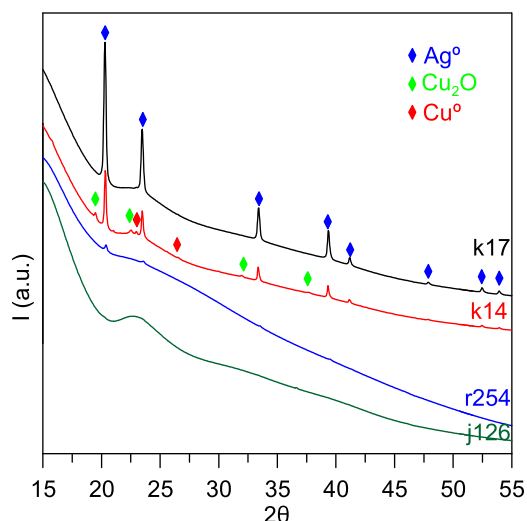
FIG. 2. SR-micro XRD of the luster layers. The high background corresponds to the glass substrate. The data show the difference in size and long range order of the silver metal nanoparticles present in the layers.

Color coordinates of the luster layers were determined from the UV-Vis reflectance spectra using the protocol accepted by the International Commission for Illumination (CIE Lab 1976). The copper lusters show a large red (positive **a**) and a smaller yellow (positive **b**) component in contrast to silver lusters, which have large yellow and a small red component. The silver-copper luster k17-brown presents small red and yellow components. K17-yellow has a small green (negative **a**) and a large yellow component and k14, which is a mixture of yellow and brown spots has a small red and a large yellow component.

The XRD patterns of the samples shown in Figure 2 display a high background corresponding to the amorphous matrix and peaks corresponding to metallic silver in different concentrations and crystallite sizes. The fact that samples k17 and k14 show narrow and very intense peaks, while the remaining samples show very small and relatively broad peaks, indicates that the silver nanoparticles are larger in the case of the mixed silver-copper samples than in the case of the pure-silver ones. By subtracting the background from the patterns of the samples k17 and k14 and measuring the peak widths, an average particle size of about 25 nm was estimated. On the other hand, the considerable amorphous background and the low intensity of the silver peaks in the diffraction patterns of the samples j126 and r254 made it impossible to obtain a reliable estimate of the particle size although it can be asserted that it should be rather smaller.

The diffraction patterns of k14 present also some additional peaks that are assigned to cuprite (Cu_2O) and metallic copper whose concentrations are estimated to be around 3–4 wt. % and 2–7 wt. %, respectively, depending on the spot measured. On the contrary, neither metallic copper nor cuprite diffraction peaks appear on the patterns of sample k17. Therefore, most of the copper can be expected to be in the form of Cu(I) or Cu(II) ions in the glass matrix, as it has
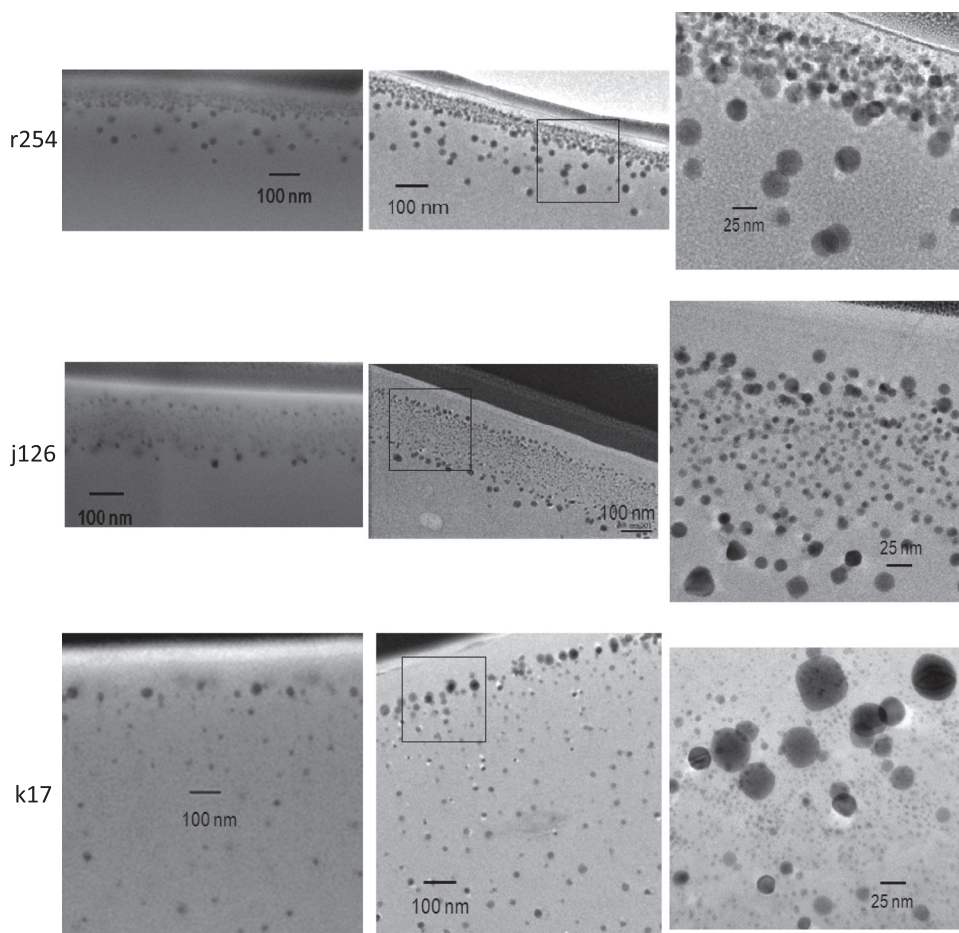

FIG. 3. SEM (left) and TEM (middle and right) images from r254 (top), j126 (middle), and k17 (bottom).

already been determined in similar lusters by EXAFS[11,12] by us and other researchers.

The existing relationship between the morphology of the materials and their aspect can be appreciated from the SEM and TEM of the silver luster, r254, and of the silver-copper luster, k17-brown, shown in Figure 3. Although the structure is similar in all the cases with a surface layer free of silver particles and below it a main silver particle containing layer, the thickness and particle size distribution of the layers are different in each case.

Sample r254 has a first 15 nm silver free layer, a 70 nm thick main layer of densely packed silver nanoparticles of 7 nm average size, and occasional larger particles (of about 20 nm) dispersed deeper in the glaze (down to 300 nm). Sample j126 shows a 50 nm first silver free layer, a second 160 nm layer comprising 4.5 nm size silver nanoparticles and scarce larger silver nanoparticles (of about 20 nm) deeper in the glaze. Finally, k17 shows a 100 nm silver free glass layer, and a main layer (several microns) containing silver nanoparticles with a very heterogeneous size, ranging from a few nanometers to 40 nm.

Thus, a first, layer made of large (30 nm) and very small (2–4 nm) nanoparticles is followed by a less concentrated layer containing 10 nm silver particles. Although the glass is copper rich, no copper containing crystalline precipitates are found. The estimation of the nanoparticles volume fraction is difficult due to the large particle overlap, especially for r254 and j126 for which the thickness of the lamellae (50–60 nm) is too large in comparison to the size of the particles. Nevertheless, it is easy to appreciate from the SEM images that the nanoparticles volume fraction for r254 is higher than for j126 and k17.

The size of the metal nanoparticles depends not only on the reducing atmosphere but also on the presence of other
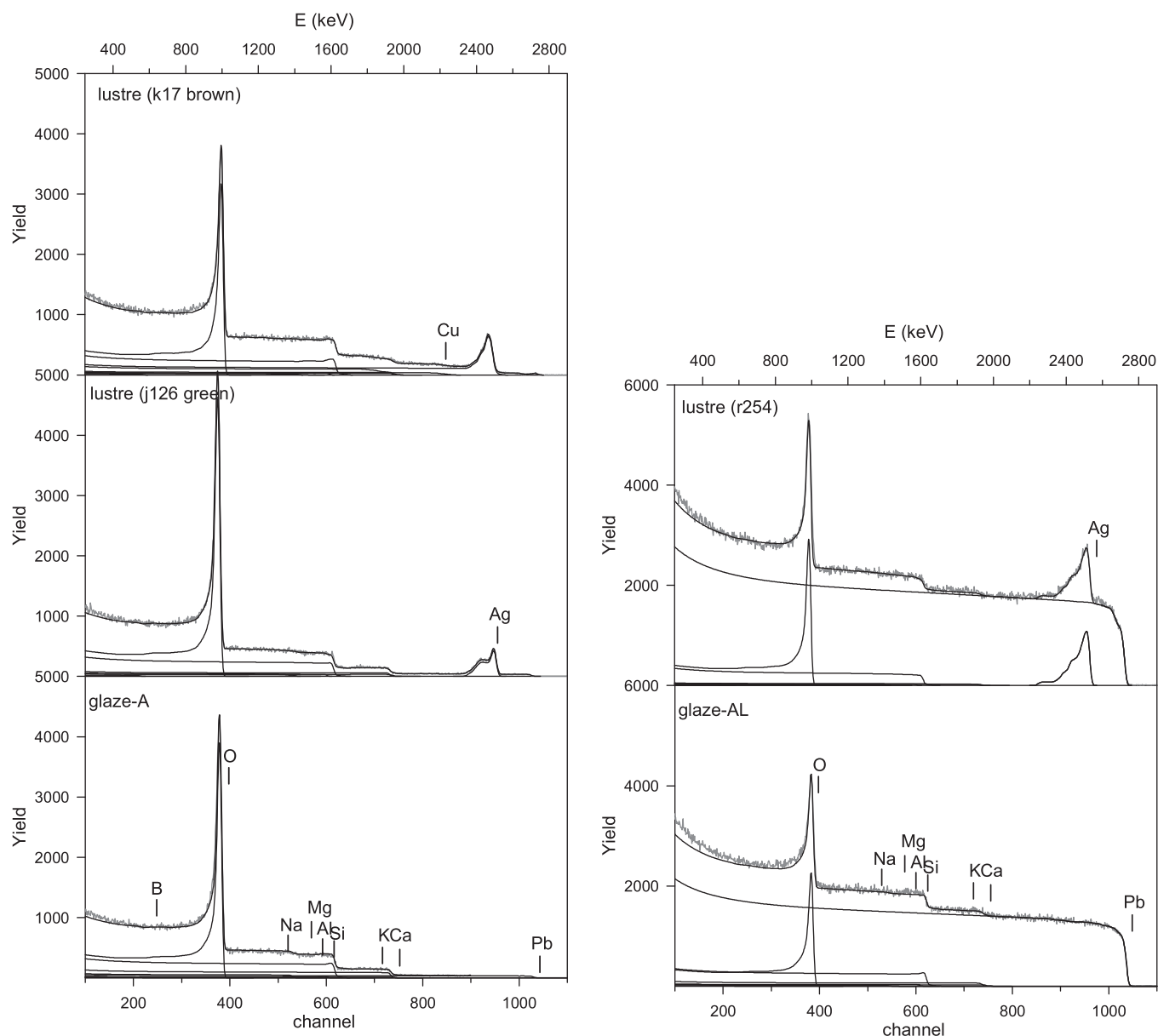

FIG. 4. Fitted RBS spectra corresponding to (left) the lead free glaze, the silver lustre j126, and the copper-silver lustre k17, (right) the lead bearing glaze and the silver lustre r254.
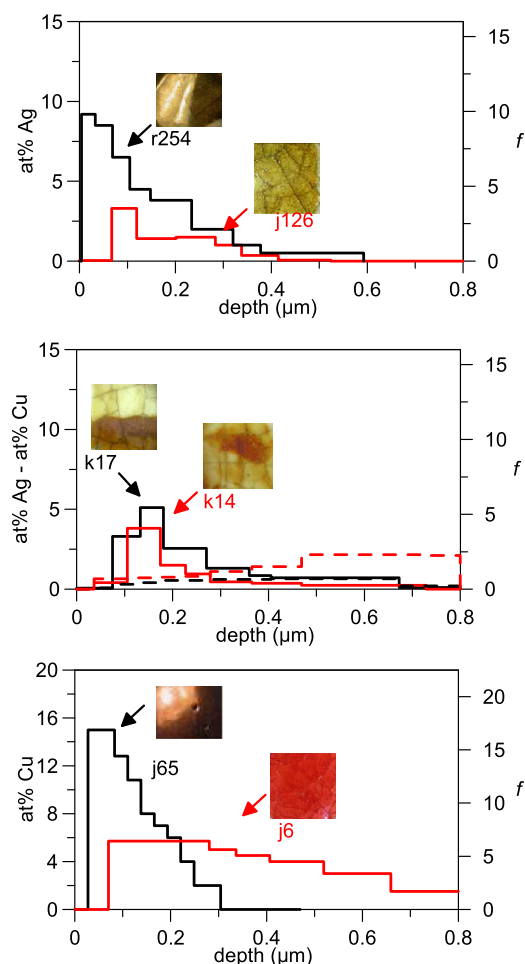
FIG. 5. (Top) Fitted silver depth profile corresponding to silver replicated lustres over lead free and lead bearing glazes, respectively, j126 (red line) and r254 (black line), (middle) fitted silver (continuous line) and copper (dashed line) depth profiles corresponding to mixed silver-copper luster produced over a lead free glaze, k17 (black line) and k14 (red line), (bottom) fitted copper depth profile from the two copper lusters produced over a lead free and lead bearing glaze, respectively, j65 (black line) and j6 (red line).[12]

reducing agents either/both in the original mixture or/and in the glass. The glass substrates studied here do not contain any reducing agent. However, in the case of the silver-copper lusters, copper acts as a reducing agent for silver, resulting in the formation of larger silver nanoparticles. It also explains why copper is present as Cu(II) or Cu(I), as happens for k17, and does not form cuprite or metalliccopper nanoparticles. Moreover, copper could also be reduced and forms cuprite and metallic copper nanoparticles, as occurs in

k14 if a stronger reducing atmosphere is applied during the synthesis.

Figure 4 shows the fitted RBS spectra used to obtain the depth-concentration profiles shown in Figure 5 corresponding to the silver and silver-copper lusters. The fitted copper spectra were published elsewhere.[17,18]

It can be seen from the plots shown in Figure 5 that the metal particles are concentrated close to the surface for the lusters obtained with the lead bearing glaze (samples r254 and j65), while in contrast they are distributed deeper inside for those lusters obtained with a lead-free glaze (samples j126, j6, k14, and k17). This is attributed to reduced silver and copper diffusivity in the lead bearing glaze giving rise to the formation of more nuclei per unit volume.

Another interesting aspect is that in the case of the silver-containing samples the metal particles are concentrated closer the surface than in the copper-containing ones; this feature, together with the fact that silver is much more easily reducible, could explain why gold-like silver lusters are more easily obtained than copper lusters. Therefore, silver is more concentrated than copper closer to the surface in the silver-copper lusters, k14 and k17. This has also been found by TEM[38] observation of historical lusters. These lusters were produced at higher temperatures and using CO instead of H_2 as the reducing gas (due to its large molecule CO has a lower permeability in the glaze than H_2). However, the results obtained indicate that the depth at which the luster layer is formed is essentially controlled by the composition of the glaze and by the fastest diffusing ion rather than by any other processing parameter (at least in the range of temperatures of the reported experiments).

The average chemical compositions obtained from the fitted profiles are shown in Table II, and a summary of the main sample characteristics is shown in Table III. The average copper and silver content ($\langle Cu \rangle$ and $\langle Ag \rangle$) in the layer, the relative percentage of copper (Cu/(Cu + Ag)), the maximum content of copper and silver (Cu_{max}, Ag_{max}), the maximum volume fraction of particles in the layer (f_{max}), the total Cu and Ag atoms by unit surface area, the depth at which the maximum of silver and copper content occur (position Ag_{max} and Cu_{max}), and the luster layer thickness are given in Table III. It can be seen from these data that only those luster layers containing a high volume fraction (about 10%) of metal particles present the metallic aspect, in perfect agreement with the results obtained for laboratory-replicated copper lusters[17] and for early silver Islamic lusters.[18] On the contrary, the metallic shine is neither related to the average

TABLE II. Average composition of the lustre layers determined from RBS fittings.

Sample	Si	O	K	Ca	Cu	Ag	Pb	Na	Mg	Al	B
j6	15.5	58.9	2.07	0.50	2.83	…	0.06	4.63	0.05	2.67	12.64
j65	17.4	58.6	1.06	0.47	6.35	…	2.52	2.12	0.07	2.92	8.25
r254	18.0	61.7	1.20	0.90	…	2.80	3.57	1.51	0.30	3.00	7.00
j126	15.9	60.6	2.20	1.23	…	0.95	0.06	3.75	0.04	2.78	12.50
K17 brown	15.6	59.9	3.17	0.90	0.47	1.41	0.06	2.32	0.20	2.60	12.32
K17 yellow	14.7	60.3	2.00	0.90	0.31	0.13	0.05	3.55	0.20	2.60	15.19
k14 brown/yellow	14.4	63.5	1.54	0.71	1.30	0.75	0.05	0.56	0.13	2.66	14.31

TABLE III. Some properties of the luster layers calculated from the fitted RBS spectra. $\langle Cu \rangle$ and $\langle Ag \rangle$ account for the average copper and/or silver content in the layer; Cu/(Cu + Ag) for the relative proportion of copper and silver; Cu_{max} and Ag_{max} for the maximum concentration in the layer; f_{max} is the maximum volume fraction of metal nanoparticles in the layer; D/d_{max} is a geometrical parameter calculated after Torquato considering a random arrangement of the nanoparticles in the layer, where D is the distance between the center of consecutive particles and d is the size of the particles. The total copper and silver atoms per square centimeter, the thickness of the layer, and the position of the maximum concentration of metal particles in the layer are also given.

Sample									Lustre layer				
Type	Reference	$\langle Cu \rangle$ at. %	$\langle Ag \rangle$ at. %	Cu/(Cu + Ag) %	Cu_{max} at. %	Ag_{max} at. %	f_{max}	D/d_{max}[a]	Total Cu $\times 10^{15}$ atm/cm^2	Total Ag $\times 10^{15}$ atm/cm^2	Position Ag_{max} nm	Position Cu_{max} nm	Thickness nm
Copper	j6	1.30	…	100	5.7	…	5.4	1.39	1990	…	…	175(35)	>1240
	j65	6.40	…	100	15.0	…	14.8	1.14	165	…	…	55(14)	249
Silver	j126	…	0.95	0	…	3.3	4.2	1.47	…	54	93(33)	…	348
	r254	…	2.80	0	…	9.2	12.5	1.18	…	104	19(2)	…	373
Copper and silver	k17 brown	0.47	1.41	25	…	5.1	6.7	1.32	21	64	157(24)	495(135)	>672
	k17 yellow	0.31	0.13	70	0.9	0.4	0.5	2.24	18	7	144(24)	>800	>600
	k14	1.30	0.75	63	2.2	3.8	4.6	1.43	57	33	140(17)	550(182)	>720

[a]Reference 39.

or total copper and/or silver content, nor to the layer position or thickness. This high concentration of metal nanoparticles is obtained by using a lead glaze, or in general modifying the glaze composition in order to reduce the mobility of silver and copper.

Among the parameters listed in Table III, we show the ratio D/d, where D is the distance between the centers of adjacent particles and d is the particle size. D/d is a geometrical parameter that gives a microscopic view of the volume fraction of nanoparticles assuming a random arrangement of the nanoparticles in the layer.[39] The maximum possible concentration of nanoparticles corresponds to $D/d = 1$ (particles are in contact). As can be seen from Table III, $D/d \approx 1.2$ for the samples presenting high reflectance, which is in agreement with previous findings.[17,18] This suggests that multiparticle interactions are responsible for the enhanced (golden and coppery) specular reflectance.

The UV-Vis diffuse reflectance spectra in $\log(1/DR)$ plot (where DR stands for the total diffuse reflectance measured by an Integrating Ulbricht sphere) representing the total light extinction are shown in Figure 6. The computed Cie-Lab color coordinates are shown in Figure 1. The spectra corresponding to j126, r254, and k17-yellow show a single broad peak at 404, 414, and 408 nm, respectively, corresponding to the SPR of the silver metal nanoparticles. The yellow-greenish color of these lusters is directly related to the position and width of the SPR peak. The k17-brown and k14 spectra show a more complex structure with a split main peak. In the k14 spectrum, a second small absorption peak at 560 nm corresponding to the presence of metal copper nanoparticles is also seen. The k17-brown spectrum shows larger splitting and broadening of the peaks than k14 and a high absorbing tail at large wavelengths (above 600 nm) most probably due to the presence of Cu(II).

It is possible to evaluate the extinction cross section of metallic silver nanoparticles in a dielectric matrix by applying the Mie theory[10] for very diluted systems. Experimental dielectric constants for the bulk metal[40] including the particle size dependence and the refractive index of the glassy matrix were used. Absorption, scattering, and extinction cross

sections may be calculated as a function of nanoparticle size and glass composition, in particular those corresponding to a lead free glass (AL, n = 1.52) are shown in Figure 7. We can see that the peak is red shifted and broadens increasing nanoparticle size. The calculated peak position (Γ_{max}) and full width at half maximum (FWHM) of the plasmon peak are also plot in Figure 7 for silver metal nanoparticles in lead free (AL, n = 1.52) and lead containing glazes (L, n = 1.58). The peak position strongly depends on the size of the nanoparticles. The values obtained for samples j126 and r254 and
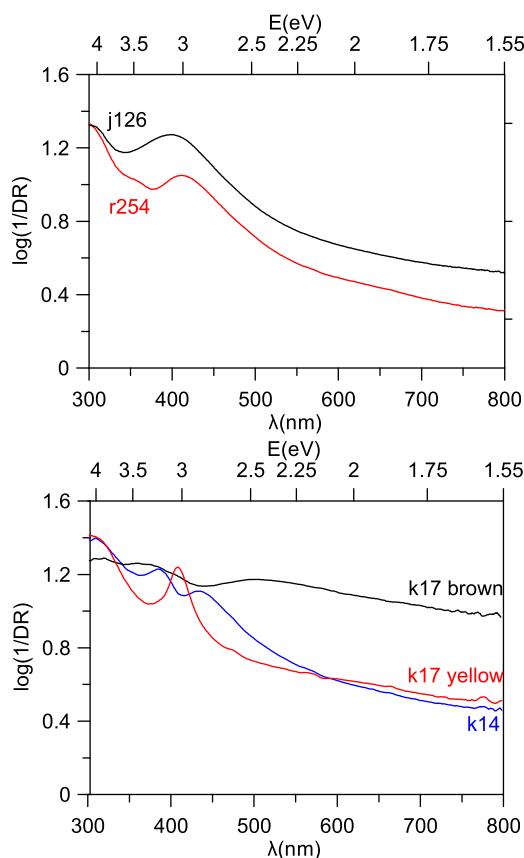

FIG. 6. UV-Vis spectra corresponding to the samples studied: (top) silver lusters, j126 and r254, (bottom) silver-copper lusters, k17 and k14.
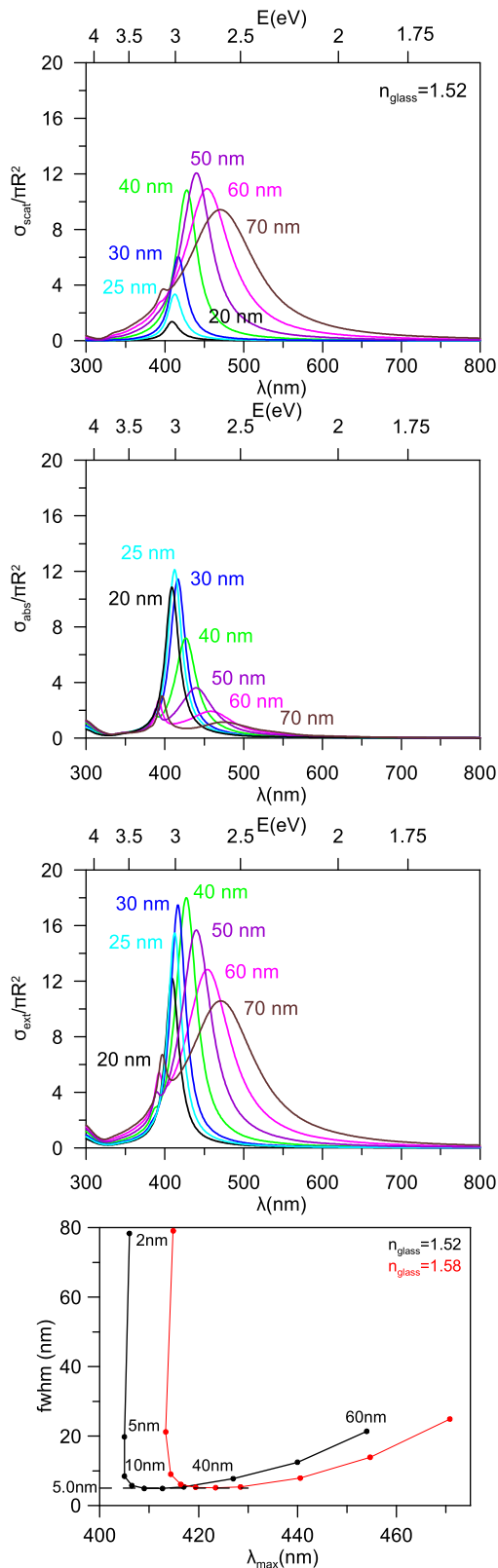
FIG. 7. From top to bottom, absorption, scattering and extension cross sections corresponding to the Mie calculations as a function of nanoparticle size for the lead free glass. At the bottom, full width half maximum versus peak position plot corresponding to silver metal nanoparticles of varying size in a lead free (black line) and a lead bearing glass (red line) calculated using the Mie theory.

k17-yellow correspond to particle sizes up to 10 nm for j126 and r254, and of about 20 nm for k17-yellow. The FWHM increases for particles smaller than 10 nm or larger than 40 nm. This explains why j126 and r254 with particles smaller than 10 nm present a very broad peak while on the contrary k17-yellow which is mainly formed by larger particles presents a narrow peak. However, the FWHM of the peaks is larger than expected even considering a broad size distribution of small particles.

Although peak splitting and large red shifts also follow from the Mie calculations for silver particles larger than 50 nm, the sizes of the nanoparticles in our brown layers are not big enough to justify the important shifts and broadening observed in the spectra corresponding to k17-brown and k14. Actually, the approximation of non-interacting spheres is not applying to any of the luster samples studied. We must then consider that the particles are not isolated, and that the color of the lusters is also affected by multiparticle collective scattering.

In order to verify the effect of multiparticle scattering in the optical response of the layers, FDTD simulations were performed and the main results from which are presented in Figure 8. The absorption and scattering spectra of clusters of relatively small-sized particles (d = 10 nm) present a clearly distinguishable plasmon resonance peak, which is much broader than expected for the single particle case described by the Mie theory. This broadening is a clear indication of collective scattering. However, the scattering contribution is small and the SPR spectrum is dominated by the absorption contribution, an observation that coincides with the predictions of Mie's theory.

In contrast, for larger silver nanoparticles (d = 30 nm), the interparticle interactions affect even more the optical response for volume fractions as small as 0.1%. Both the absorption and scattering spectra broaden towards the long wavelengths with increasing particle concentration but the scattering intensity increase towards the red end of the spectrum is especially pronounced. The extinction cross section is therefore dominated by the scattering contribution even for moderate volume fractions of particles. The spectrum is very broad and the dipolar plasmonic contribution becomes hardly distinguishable.

In summary, both j126 and r254 are formed by very small silver nanoparticles and therefore the golden shine effect shown by r254 cannot be related to the presence of large nanoparticles. In both cases, a silver free surface glassy layer followed by a silver nanoparticle-bearing layer is found. The thicknesses of the layers for r254 (25 and 70 nm) are half than those of j126 (50 nm and 180 nm). However, the particles are too small and the layers are too thin to produce a multi-layered interfering structure in the visible. On the contrary, the results confirm the need of dense nanoparticulated layers where interparticle interactions enhance the coherent scattering of light.

Concerning the blue specular reflectance shown by k17-brown, as particle size increases the scattering coefficient increases in the wavelength range where the SPR happens (between 405 and 415 nm). Moreover, increasing the incident angle, the specular reflectance also increases. Therefore, the presence of an upper very low density layer of large
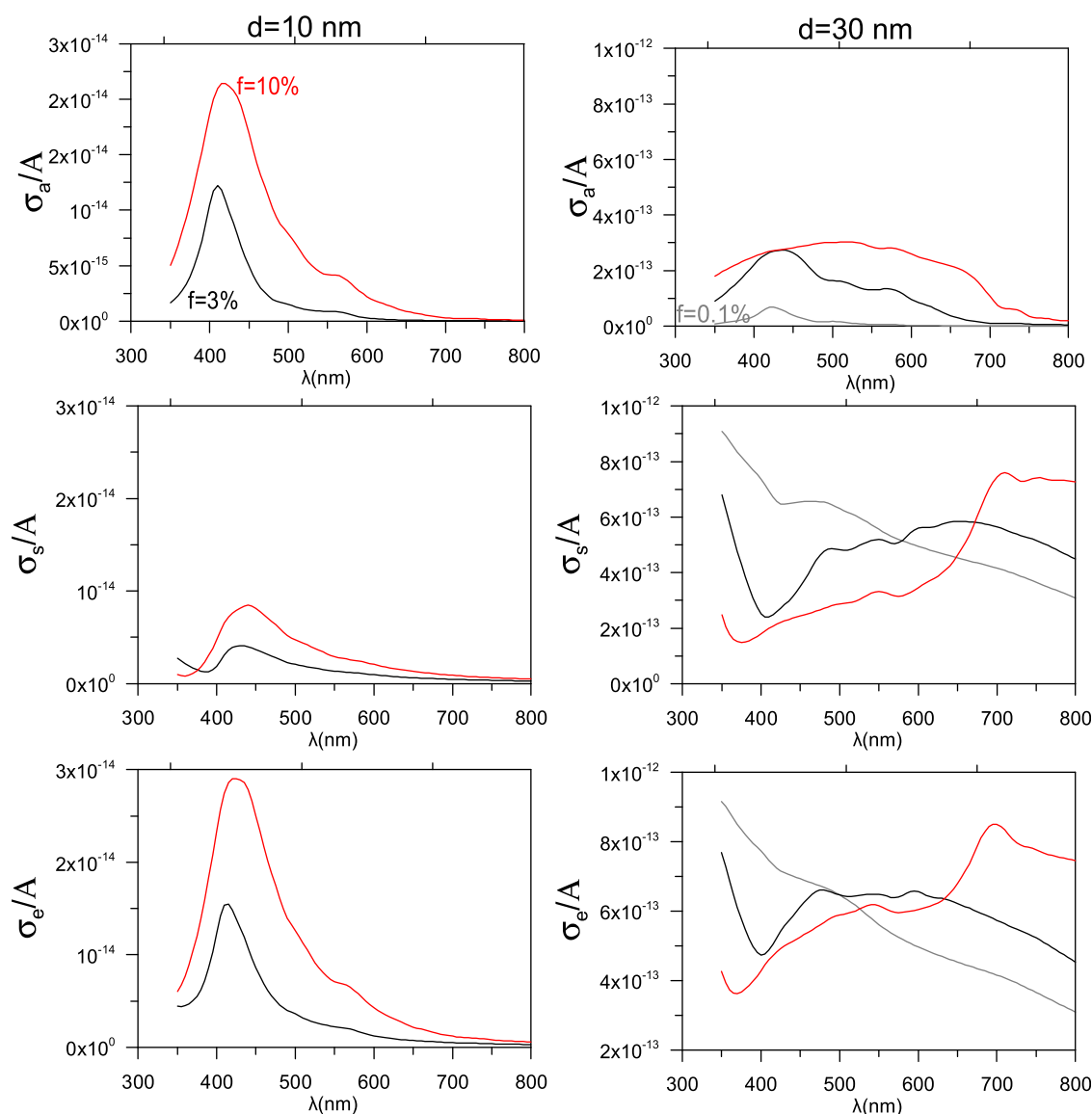
FIG. 8. From top to bottom, simulated absorption, scattering, and extinction cross section plots corresponding to 3% (black line) and 10% (red line) volume fraction of silver nanoparticles of (left) 10 nm and (right) 30 nm size.

nanoparticles (30 nm) is expected to produce a blue specular reflectance, especially at high incident angles. The presence of very small nanoparticles will not affect the reflectance as both absorption and scattering are two orders of magnitude smaller. A similar nanostructure obtained by ion implantation[41] produced the same blue specular reflectance.

Finally, sample k14 shows a two layered structure of large nanoparticles. The first, closer to surface, contains mainly silver nanoparticles while the second, 500 nm below the surface, contains mainly copper and cuprite nanoparticles. The absorption and scattering of silver and copper nanoparticles do not overlap (410 nm and 560 nm, respectively). In this case, scattering and absorption contributions of large silver and copper particles combined are responsible for the purple color observed.

IV. CONCLUSIONS

The study of a selection of silver and silver-copper luster layers designed to have similar particle sizes and layer thicknesses but different silver nanoparticle concentrations has clarified the reasons for the golden like shine and colour shown by the layers. Neither the large size of the particles nor the particular alternated silver-free and silver-bearing layered structure is responsible for the increased reflectance shown by some of them; on the contrary, the high volume fraction of metal nanoparticles is found to be decisive for the metallic like effect. This is mainly correlated to the reduced diffusivity of silver and copper in the lead bearing glaze compared to the lead free glaze, and less to the production parameters (atmosphere, temperature, composition). On the contrary, the colour shown by the layers is directly related to the size distribution of the particles in the layers and therefore to the composition but also to the production parameters. The simultaneous introduction of copper and silver improves the growth of the silver nanoparticles and at the same time diminishes the precipitation of metal copper nanoparticles. Copper diffuses further than silver helping the formation of thicker luster layers with silver richer and copper richer areas. Copper is mainly kept as Cu II unless a strong

reducing external atmosphere is used; then cuprite and metallic copper nanoparticles are formed.

As a global outline of the luster production process, we have shown that the metallic shining effect is mainly controlled by the diffusivity of metallic ions in the glass substrate, while colour is mostly dependent on the relative concentrations of Ag and Cu in the initial mixture and on the processing parameters, i.e., thermal protocol and reducing agent.

ACKNOWLEDGMENTS

[1]J. Pérez-Arantegui, J. Molera, A. Larrea, T. Pradell, M. Vendrell, I. Borgia, B. G. Brunetti, F. Cariati, P. Fermo, M. Mellini, A. Sgamellotti, and C. Viti "Luster pottery from the thirteenth century to the Sixteenth century: a nanostructured metallic thin metallic film," J. Am. Ceram. Soc. **84**(2), 442–446 (2001).

[2]I. Borgia, B. Brunetti, I. Mariani, A. Sgamellotti, F. Cariati, P. Fermo, M. Mellini, C. Viti, and G. Padeletti, "Heterogeneous distribution of metal nanocrystals in glazes of historical pottery," Appl. Surf. Sci. **185**, 206–216 (2002).

[3]S. Padovani, C. Sada, P. Mazzoldi, B. Brunetti, I. Borgia, A. Sgamellotti, A. Giullvi, F. D'Acapito, and G. Battaglin, "Copper in glazes of Renaissance luster pottery: Nanoparticles, ions, and local environment," J. Appl. Phys. **93**(12), 10058–10063 (2003).

[4]P. Colomban, "The use of metal nanoparticles to produce yellow, red and iridescent color, from bronze age to present times in luster pottery and glass: Solid state chemistry, spectroscopy and nanostructure," J. Nano Res. **8**, 109–132 (2009).

[5]A. Caiger Smith, *Luster Pottery* (New Amsterdam Books, New York, 1991).

[6]R. B. Mason, *Shine Like the Sun: Luster-Painted and Associated Pottery From the Medieval Middle East, Bibliotheca Iranica: Islamic Art and Architecture Vol. 12* (Mazda, Costa Mesa, Canada, 2004).

[7]J. Molera, C. Bayés, P. Roura, D. Crespo, and T. Pradell, "Key parameters in the production of medieval luster colors and shines," J. Am. Ceram. Soc. **90**(7), 2245–2254 (2007).

[8]G. Padeletti, P. Fermo, A. Bouquillon, M. Aucouturier, and F. Barbe, "A new light on the first exemple of lustred majòlica in Italy," Appl. Phys. A **100**, 747–761 (2010).

[9]J. Molera, M. Mesquida, J. Perez-Arantegui, T. Pradell, and M. Vendrell, "Luster recipes from a medieval workshop in Paterna," Archaeometry **43**(4), 455–460 (2001).

[10]U. Kreijig and M. Vollmer, *Optical Properties of Metal Cluster*, Springer Series in Materials Science Vol. 25 (Springer Verlag, Berlin, 1995).

[11]S. Padovani, I. Borgia, B. Brunetti, A. Sgamellotti, A. Giullvi, F. D'Acapito, P. Mazzoldi, C. Sada, and G. Battaglin, "Silver and copper nanoclusters in the luster decoration of Italian Renaissance pottery: An EXAFS study," Appl. Phys. A **79**(2), 229–233 (2004).

[12]A. D. Smith, T. Pradell, J. Roque, J. Molera, M. Vendrell-Saz, A. J. Dent, and E. Pantos, "Color variations in 13th century hispanic lustre—An EXAFS study," J. Non-Cryst. Solids **352**, 5353–5361 (2006).

[13]J. C. M. Garnett, Philos. Trans. R. Soc. London **203**, 385 (1904); **205**, 237 (1906).

[14]I. Farbman, O. Levi, and S. Efrima, "Optical response of concentrated colloids of coinage metals in the near-ultraviolet, visible and infrared regions," J. Chem. Phys. **96**(9), 6477–6485 (1992).

[15]P. E. Wolf and G. Maret, Phys. Rev. Lett. **55**(24), 2696–2699 (1985).

[16]Y. Kuga and A. Ishimaro, J. Opt. Soc. Am. **1**(8), 831–835 (1984).

[17]T. Pradell, A. Climent-Font, J. Molera, A. Zucchiatti, M. D. Ynsa, P. Roura, and D. Crespo, "Metallic and non-metallic shine in luster: An elastic ion backscattering study," J. Appl. Phys. **101**(9), 103518 (2007).

[18]P. C. Gutierrez, T. Pradell, J. Molera, A. D. Smith, A. Climent-Font, and M. S. Tite, "Color and golden shine of silver islamic luster," J. Am. Ceram. Soc. **93**(8), 2320–2328 (2010).

[19]J. Roqué, J. Molera, P. Sciau, E. Pantos, and A. Vendrell-Saz, J. Eur. Ceram. Soc. **26**, 3813 (2006).

[20]C. Mirguet, P. Frederick, P. Sciau, and P. Colomban, Phase Transitions **81**(2–3), 253–266 (2008).

[21]V. Reillon and S. Bethier, "Modelization of the optical colorimetric properties of lustred ceramics," Appl. Phys. A **83**, 257–265 (2006).

[22]P. Sciau, C. Mirguet, C. Roucau, D. Chabanne, and M. Schvoerer, "Double nanoparticle layer in a 12th century lustreware decoration: Accident or technological mastery?," J. Nano Res. **8**, 133–139 (2009).

[23]J. Roqué, N. R. J. Poolton, J. Molera, A. D. Smith, E. Pantos, and M. Vendrell-Saz, "X-ray absorption and luminescence properties of metallic copper nanoparticles embedded in a glass matrix," Phys. Status Solidi B **243**, 1337–1346 (2006).

[24]A. Taflove and S. Hagness, *Computational Electrodynamics: The Finite-Difference Time-Domain Method*, 3rd ed. (Arctech, Norwood, MA, 2005).

[25]T. Pradell, J. Molera, E. Pantos, A. D. Smith, C. M. Martin, and A. Labrador, "Temperature resolved reproduction of medieval luster," Appl. Phys. A **90**(1), 81–88 (2008).

[26]A. Fluegel, "Global model for calculating room-temperature glass density from the composition," J. Am. Ceram. Soc. **90**(8), 2622–2625 (2007).

[27]A. I. Priven and O. V. Mazurin, "Comparison of methods used for the calculation of density, refractive index and thermal expansion of oxide glasses," Glass. Technol. **44**(4), 156–166 (2003).

[28]W. K. Chu, J. W. Mayer, and M. A. Nicolet, *Backscattering Spectrometry* (Academic, New York, 1978).

[29]A. Climent-Font, F. Pászti, G. García, M. T. Fernández-Jiménez, and F. Agulló, "First measurements with the Madrid 5 MV tandem accelerator," Nucl. Instrum. Methods Phys. Res. B **219-220**, 400–404 (2004).

[30]C. Huan-Sheng, S. Hao, T. Jiayong, and Y. Fujia, "Cross sections for 170 backscattering of 4He from oxygen in the energy range of 2.0-9.0 MeV," Nucl. Instrum. Methods Phys. Res. B **83**, 449–453 (1993).

[31]M. Mayer, "SIMNRA user's guide," IPP 9/113, 1997.

[32]R. Jarjis, "Ion beam archaeometry of Islamic luster glaze," Key Eng. Mater. **132-136**, 1434–1437 (1997).

[33]D. Hélary, "Études de couches dorées sur matières vitreuses: Aplications aux tesselles à feuille d'or et aux céramiques glaçurées à décors de lustres dorés," Thesis (Docteur de l'Ecole des Mines de Paris, Spécialité Science et Génie des Matériaux, 2003).

[34]G. Padeletti, G. M. Ingo, A. Bouquillon, S. Pages-Camagne, M. Aucouturier, S. Roeres, and P. Fermo, "First-time observation of Mastro Giorgio masterpieces by means of non-destructive techniques," Appl. Phys. A **83**, 475–483 (2006).

[35]See http://www.lumerical.com for FDTD Solutions, Lumerical Solutions, Vancouver, Canada.

[36]K. Yee, IEEE Trans. Antennas Propag. **14**(3), 302–307 (1966).

[37]E. D. Palik, *Handbook of Optical Constants of Solids* (Academic, New York, 1998).

[38]P. Fredrickx, D. Hélary, D. Schryvers, and E. Darque-ceretti, "A TEM study of nanoparticles in lustre glazes," Appl. Phys. A **79**, 283–288 (2004).

[39]S. Torquato, "Nearest-neighbor statistics for packing hard spheres and disks," Phys. Rev. E **51**(4), 3170–3182 (1995).

[40]P. B. Johnson and R. W. Christy, "Optical constants of noble metals," Phys. Rev. B **6**(12), 4370–4379 (1972).

[41]R. H. Magruder, S. J. Robinson, C. Smith, A. Meldrum, A. Halabaica, and R. F. Haglund, "Dichroism in Ag nanoparticle composites with bimodal size distribution," J. Appl. Phys. **105**, 024303-1-5 (2009).